JOURNAL OF MATERIALS SCIENCE 27 (1992) 5720–5726

Microstructural characterization of "white zones" in weldable 7000 series alloys

W. HEPPLES, M. C. THORNTON, N. J. H. HOLROYD
Alcan International Ltd, Southam Road, Banbury, Oxon OX16 7SP, UK

Previous attempts using electron metallographic techniques to study the microstructures of aluminium alloy weldments have been limited by the artefacts introduced by conventional preparation methods such as electropolishing or ion-beam thinning and by difficulties in precisely locating microstructural regions of critical interest in the electron-transparent areas of specimens. This paper describes how microtomy has minimized these problems for the characterization of interfacial regions in AlZnMg alloy weldments that can be susceptible to environment-sensitive fracture. Regions of interest were identified by a linear trace of microhardness indentations on a specimen mechanically polished to a 0.25 μm finish. This surface was examined in the scanning electron microscope using backscattered electrons to relate the region of interest to specific hardness indentations. Foils for transmission electron microscopy were then microtomed from an area adjacent to the appropriate hardness indentation. Microstructural analysis of the white zone region has been made, using secondary and backscattered electron imaging, transmission electron microscopy, X-ray microanalysis and electron probe microanalysis. The transfer of intermetallics during the welding process to grain boundary regions from intragranular sites, and the segregation of zinc, magnesium and copper (10.0, 3.5 and 0.3 wt % respectively) to grain boundary regions, has been quantified and is briefly discussed with respect to stress corrosion cracking of other AlZnMg (Cu) alloys.

1. Introduction

Medium-strength weldable aluminium alloys (7000 series) are stronger than other weldable alloys such as Al–Mg or Al–Mg–Si and when welded offer the unique advantage of naturally age-hardening heat-affected zones [1]. Commercial exploitation of these alloys has been restricted by service experience of localized corrosion [1–4], although recent developments should alleviate these problems [5–8]. Localized corrosion generally occurs as exfoliation corrosion within the heat-affected zone a few millimetres from the weld bead or as a type of stress corrosion cracking known as weld-toe cracking or white zone cracking [1–12]. Cracking initiates at weld-toes and propagates intergranularly into the interfacial region between the weld-bead and the heat-affected zone, commonly known as the "white zone" due to its etching behaviour in nitric acid [9, 10].

The white-zone region has been the subject of several microstructural investigations involving both optical and electron metallographic techniques [3, 9–12]. However, sample preparation of white-zone material has presented severe experimental difficulties. In studies to date, foils for transmission electron microscopy (TEM) have been prepared from 3 mm diameter discs punched out from appropriate regions and thinned by either selective electro-polishing or ion-beam thinning techniques. These two methods have the following disadvantages. For selective electropolishing they are

(a) difficulty in masking the desired area due to the size of the white zone;
(b) because of electrochemical variations in the region of the weld–parent metal interface, thinning of the desired location has been unpredictable; and
(c) the electrolytes used are aggressive towards the microstructure.

For ion-beam thinning they are

(a) limited accuracy in thinning precise locations, and
(b) the introduction of artefacts.

1.1. Ultramicrotomy

Ultramicrotomy can be used to provide thin foils for TEM and corresponding bulk samples that can be used for electron probe microanalysis (EPMA) and back-scattered electron imaging (BEI). These foils can be accurately taken from a precise location with minimal electrochemical damage and the problems encountered in previous studies can be overcome. Hence this form of specimen preparation has allowed the complete microstructural characterization of the white zone.

0022–2461

2. Experimental procedure

2.1. Materials

Welded material was prepared by laying a bead-on-plate weld in the long-transverse direction on 1 m lengths of 15 mm thick 7017-T651 plate using automated MIG welding with the following parameters: 342A 28 V, 0.62 m min^{-1} traverse rate, 10 m min^{-1} wire feed rate, 10 mm nozzle height and NG61 welding wire (1.6 mm dia.). The measured compositions, determined using spectrographic analysis, of the 7017-T651 plate, commercial NG61 filler-wire and typical values for weld-beads (bead-on-plate) are quoted in Table I.

2.2. Specimen preparation

Transverse sections containing welds were cut from the welded plate and metallographically polished to a 0.25 μm diamond finish. To precisely extract samples from the white zone, without using detrimental etching, the following preparation route was used:

1. Reference points were made by a series of microhardness indentations (typically 40 indents) at 50 μm intervals traversing the weld bead, white zone and parent plate; the white zone and corresponding indents were readily identified in the scanning electron microscope when using BEI (Fig. 1).
2. The indent closest to the region of interest was noted and a square-faced rod, to include all of the indents, (~ 2 mm × 2 mm × 10 mm) was rough-cut from the welded material, using a jeweller's saw.
3. The specimen rod was then mounted in a microtome (Reichart Ultracut) and cut to shape using a glass knife while being continually monitored using stereo binoculars (60 ×). The cutting continued until a 30° pyramid with its apex being a point adjacent to the selected indent had been produced.
4. Samples normal to the pyramid apex were then removed using a diamond-knife, set to produce foils ~ 150 nm thick. These floated from the knife on a water meniscus (distilled water) for collection as quickly as possible onto carbon-coated nylon grids. The procedure for specimen preparation is diagramatically represented in Figure 2.
5. The matching bulk section was retained for high-resolution electron microscopy and microanalysis as the surface quality is superior to samples produced by conventional polishing techniques (Fig. 3).

2.3. Microstructural analysis

Backscattered electron imaging of the microtomed bulk sample was carried out using a Jeol T300 SEM.

TABLE I General composition of 7017-T651 plate, filler-wire and weld bead

Material	Composition (wt %)				
	Zn	Mg	Cu	Fe	Si
7017-T651, plate	4.9	2.3	0.14	0.38	0.20
NG61, filler-wire	0.2	5.2	0.01	0.18	0.09
Weld bead	2.9	3.3	0.07	0.18	0.09

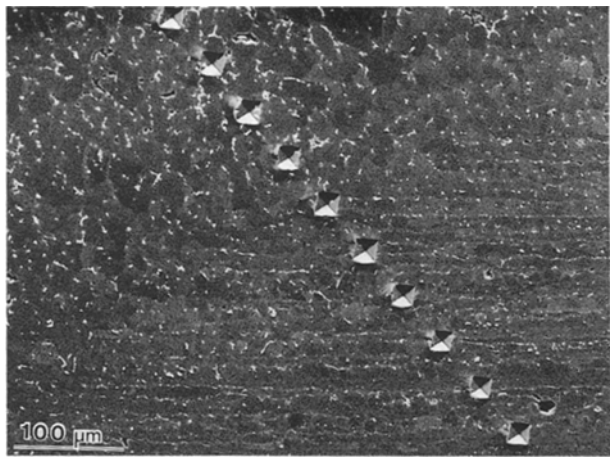

Figure 1 Backscattered electron image of a white zone traversed with microhardness indentations.

Qualitative analyses of coarse intermetallics were obtained using the Link Systems microanalysis attachment.

Quantitative EPMA was carried out on the bulk sample using a Jeol 733. Quantitative analyses of fine precipitates and grain boundaries were conducted using a Jeol 2000 FX TEM fitted with a Link Systems analyser (AN 10/25). A probe size of 50 nm was used with a minimum live-time of 200 s.

3. Results

3.1. Scanning electron metallography

High-resolution backscattered imaging of the white-zone bulk section reveals continuous dark grain boundaries, decorated with fine precipitates and adjacent diffuse regions which appear brighter (Fig. 4). The high BEI signal from the diffuse regions indicates a high mean atomic number with respect to the matrix, whereas the dark boundary indicates a lower mean atomic number. Taking care to avoid grain boundary precipitates, compositional step analyses were carried out at 1 μm intervals across grain boundaries using the EPMA (the probe size of 1 μm encompassed the whole grain boundary region). Concentration profiles obtained were consistent and showed an increase in zinc, magnesium and copper at the grain boundary with a corresponding depletion in aluminium. Fig. 5 displays the results for a scan across two grain boundaries: magnesium increased from 2.1% in the matrix to 3.4–3.6% at the grain boundary, whilst zinc increased from 5.1% to 7.0–8.1% and copper from 0.2% to 0.3%. The individual regions of the grain boundary, and the many small precipitates, were too small for accurate analyses using the microprobe, and were examined in detail using TEM.

3.2. Transmission electron metallography

The thin foils obtained via ultramicrotomy were notable for their large areas of uniform thickness. At low magnification, bands of diffraction contrast due to deformation introduced during microtomy were

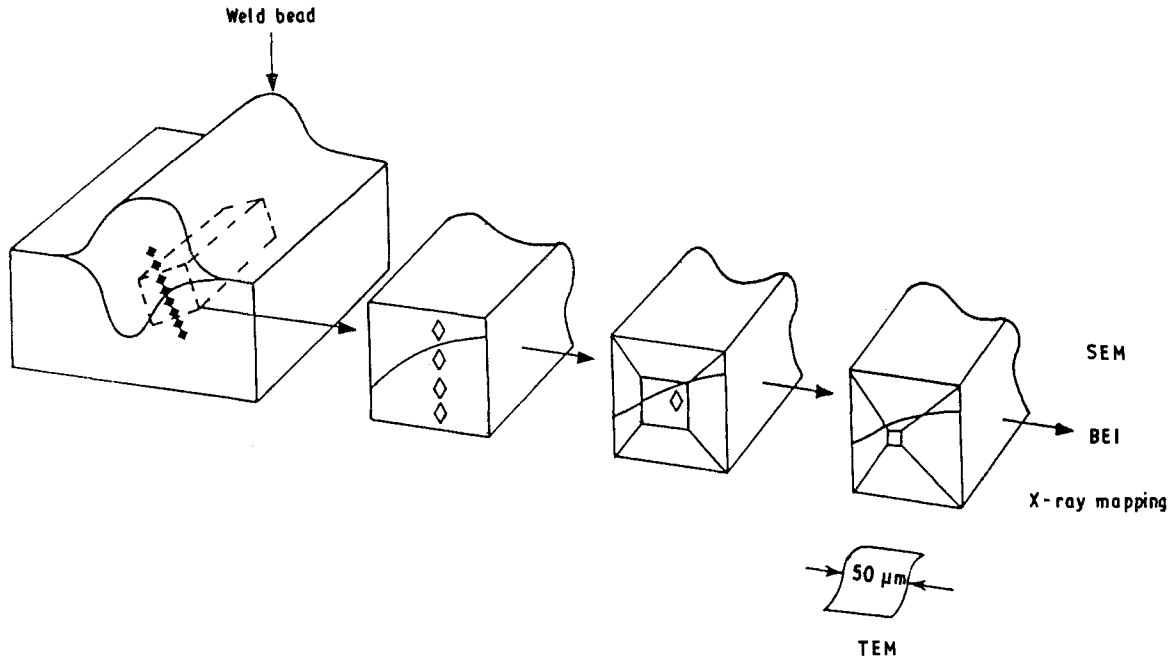

Figure 2 Sketch illustrating sample preparation.

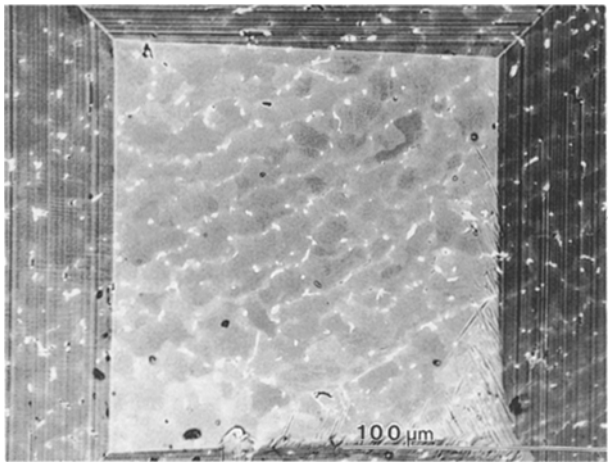

Figure 3 Backscattered electron image of microtomed sample.

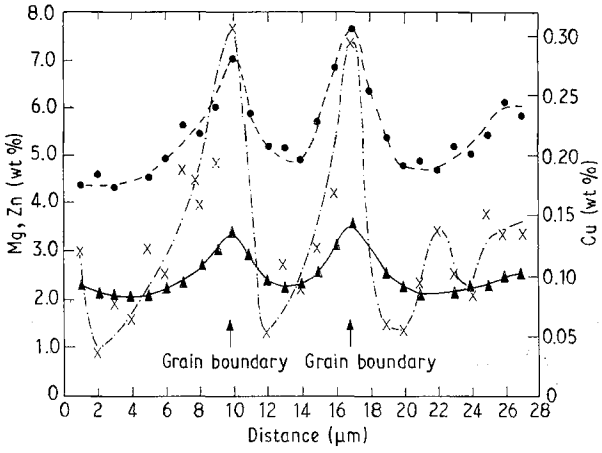

Figure 5 Step-scan across white-zone grain boundaries on bulk sample: (———, ▲) Mg, (– – –, ○) Zn, (–·–, ×) Cu.

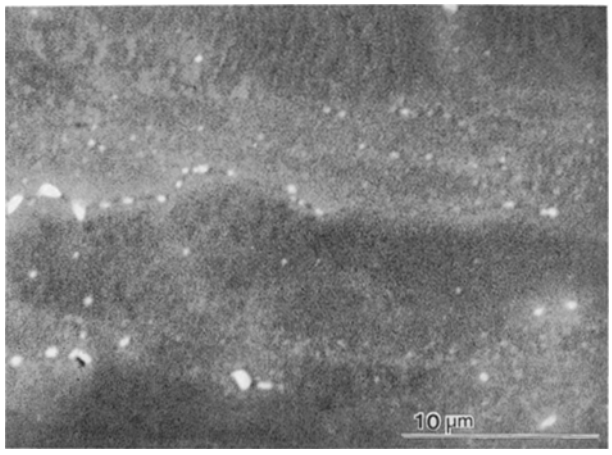

Figure 4 High-resolution backscattered electron image of the bulk sample.

readily visible, but grain boundaries and precipitates were easily discriminated (Fig. 6).

Initial assessment of the microtomed foils, obtained from a typical white-zone region, revealed an absence of matrix precipitates in agreement with the results of other workers (particularly Cordier *et al.* [9], who stated that precipitates present in the matrix before welding were swept to the grain boundary during the welding operation). Analyses obtained from the matrix were consistent with those obtained from similar areas within the bulk sample.

The white-zone grain boundaries revealed a non-uniform structure. Various types of precipitate were present which included small angular precipitates (100–200 nm), long grain-boundary stringers and agglomerations containing several different types of precipitate (Fig. 7). Typical EDAX analyses obtained from grain boundary precipitates are listed in Table II. Despite the deformation introduced during preparation of the foils, it was also possible with care to obtain diffraction patterns from some precipitates (Fig. 7). The highly reactive nature of the white-zone region was evident as examination of the grain boundaries in more detail revealed that some corrosion had occurred which was always associated with specific

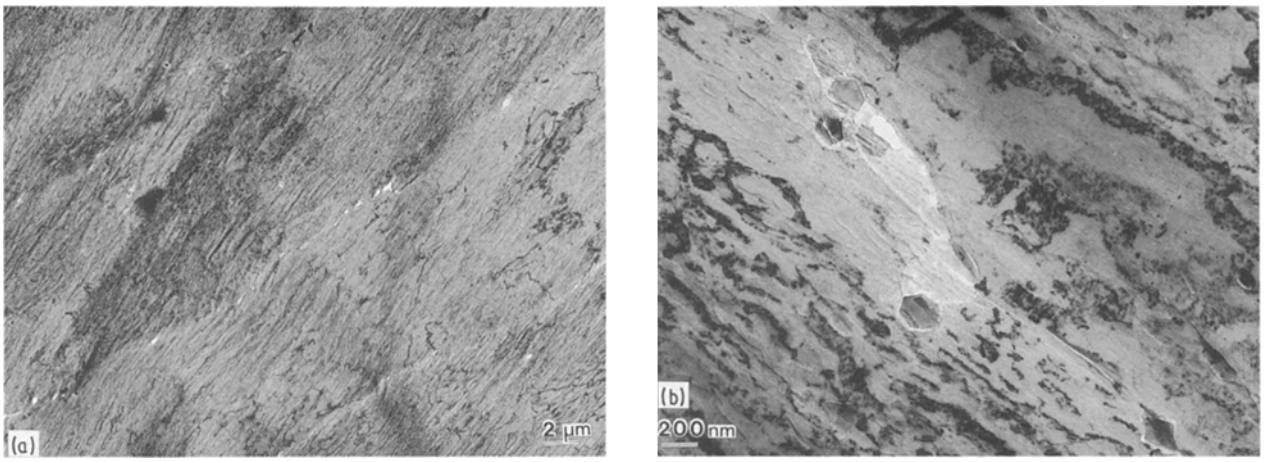

Figure 6 (a) Low-magnification view of a typical microtomed thin foil section; (b) white-zone grain-boundary region.

TABLE II Compositional ranges of white-zone grain-boundary precipitates obtained using TEM

I.D.	Composition (wt %)									Description
	Al	Zn	Mg	Cu	Fe	Mn	Cr	Si	Zr	
A	23–26	43–47	14–20	5–9	–	–	–	–	–	Stringers and irregular size and shaped precipitates
B	53–55	–	–	–	19–22	7–11	7–11	7–9	–	Both coarse and fine precipitates of the same compositions. Coarse: up to 1 μm primary intermetallics. Fine: ~ 200 nm formed during welding.
C	~ 20	–	–	–	–	–	–	~ 80	–	Amorphous phase surrounding precipitates and spreading along grain boundaries.
D	71	–	–	–	–	–	–	–	29	Equiaxed precipitates. 100 μm
White-zone Matrix	92–94	3–4	2–3	0.1	Trace elements					
White-zone grain boundary	87	8.5–9.5	3–4	0.5–0.8	–	–	–	–	–	Viscinity adjacent to G. B. (= 200 nm) away from precipitates.

types of precipitates (Figs 7 and 8). The precipitates rich in iron (precipitate 1 in Fig. 8) and those rich in zinc were found to be surrounded by corrosion whilst those precipitates which were silicon-rich (precipitate 2 in Fig. 8) were themselves corroded (corrosion surrounding precipitate 2 in Fig. 8 was caused by an adjacent zinc-rich precipitate).

A silicon-rich phase was not expected to be present in these particular alloys and in view of the associated corrosion further investigations were made. Some of these precipitates were quite large and it was possible to match the thin foils with the corresponding bulk samples (Fig. 9). It was found that the silicon-rich precipitates in the microtomed foil contained magnesium concentrations consistent with the Mg_2Si phase when analysed in the bulk sample. This suggested that the majority of the magnesium present initially in the precipitates was dissolved from the thin foil sample in a very short period of time (less than 10 s exposure to distilled water). Comparison of the matrix analyses revealed that the loss of magnesium (or other elements) was not general and the marginal loss was dependent upon its morphological state, i.e. magnesium loss only occurred from Mg_2Si precipitates. Grain-boundary step analyses away from precipitates were therefore not thought to be subject to magnesium losses. Analyses carried out at 100 nm intervals

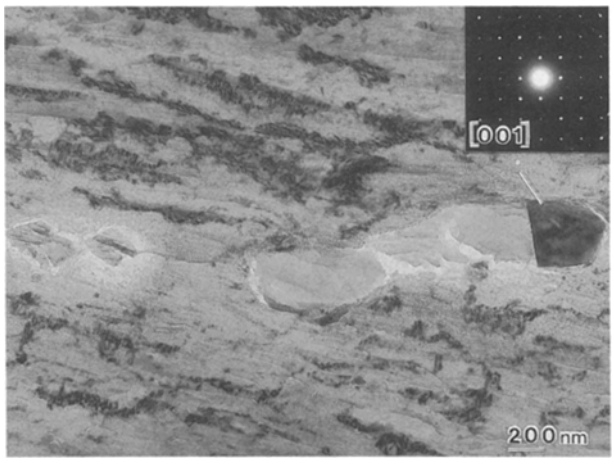

Figure 7 White-zone grain boundary showing an agglomeration of precipitates.

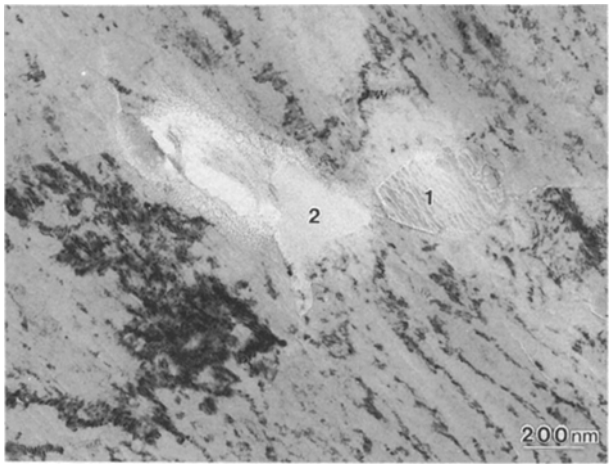

Figure 8 Micrograph exhibiting corrosion of grain-boundary precipitates: (1) Fe-rich phase, (2) Si-rich phase.

showed concentration increases in zinc, magnesium and copper across the whole grain-boundary region with respect to the matrix. However, the increased resolution available suggested that peak concentrations did not occur on the grain boundary itself, but at a distance of 200 nm to either side. The maximum concentrations measured for zinc, magnesium and copper approached 10, 4 and 0.4% respectively (Fig. 10).

4. Discussion

Backscattered electron imaging shows that the white zone consists of essentially equiaxed grains which become elongated as the parent plate is approached. In agreement with Cordier *et al.* [9], the white-zone matrix has very few precipitates and large intermetallics which were originally within the grains of the parent plate now appear at the grain boundaries. The apparent movement of precipitates has been brought about by the fact that the white zone, which was initially parent plate material, has been rapidly heated to temperatures approaching the solidus and then rapidly quenched. The solidus is exceeded at the grain boundaries and partial liquation occurs. The proximity of all precipitates to the grain boundaries demonstrates that they are either swept along by the boundaries or act as sites for grain-boundary pinning [9].

In backscattered electron imaging the white-zone grain boundaries appear diffuse with a width of 1–2 μm whereas analyses obtained from the electron microprobe suggest that the segregation in the grain-boundary region is in fact wider (~ 6 μm). It is thought that the apparent grain boundary widths suggested by the EPMA are inaccurate due to the probe size (1 μm dia.), and the sub-surface elastic scattering of electrons within the sample. However, the concentrations of zinc and magnesium (and copper) recorded in the present study are greater than those measured by other workers [9–12]. It is also considered that the concentrations of zinc and magnesium, 8.0 and 3.2% respectively, measured using the EPMA are conservative values due to beam spreading. Concentrations of zinc and magnesium, measured using microanalysis of thin foils, were significantly greater (10.0% Zn and 3.5% Mg). Grain-boundary region size was variable but the dimension shown in Fig. 10 was typical, i.e. 1200 nm. This width is in agreement with the backscattered electron images and with Schmiedel and Gruhl [11] who carried out work on simulated white-zone grain boundaries. Unlike the results from the EPMA, peak concentrations of magnesium and zinc were observed away from the centre of the grain boundary, at a distance of approximately 200 nm. Confirmation of these findings is displayed in the backscattered electron image in Fig. 4, where the centre of the grain boundary appears darker than the adjacent area.

Direct comparison with previous work is difficult, as most other investigations used post-weld-aged material [9, 10] whereas the work carried out here was on

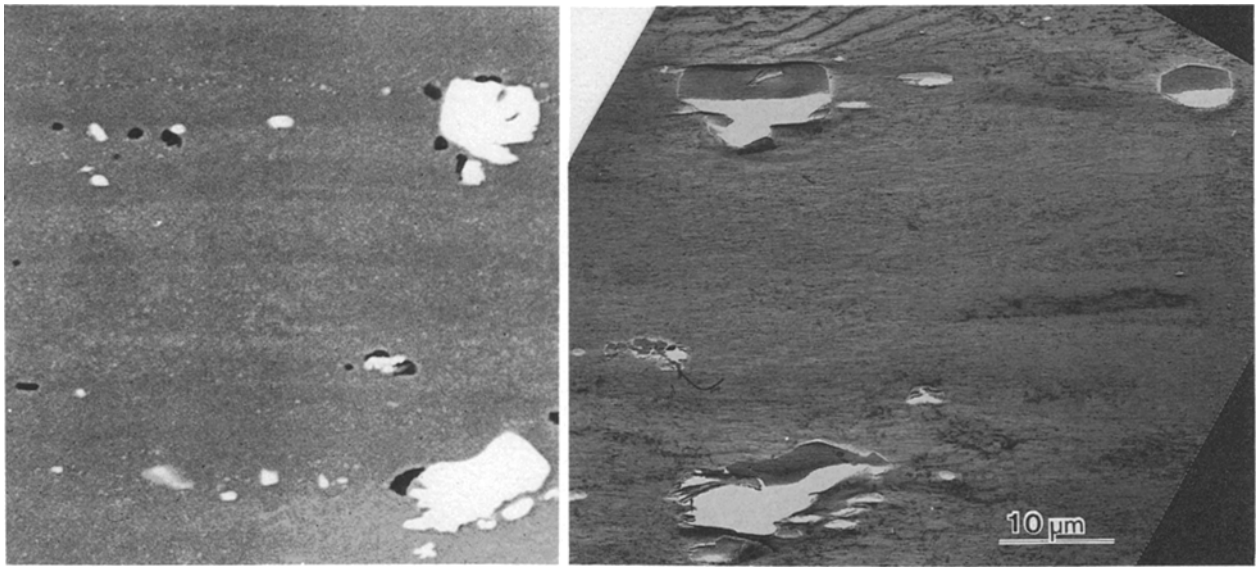

Figure 9 Comparison of precipitates in bulk and thin foil samples: (a) bulk sample, (b) thin foil.

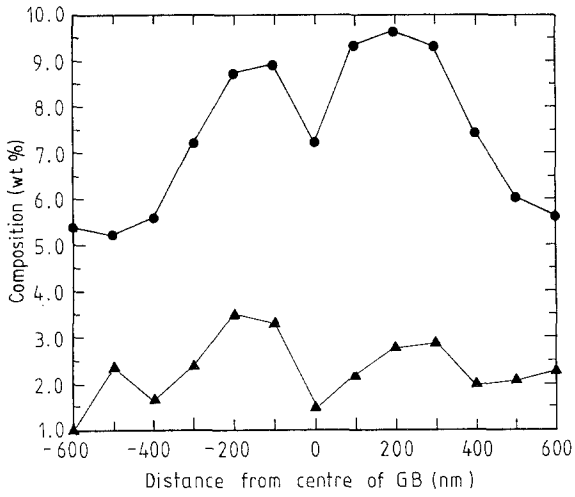

Figure 10 Step-scan across white-zone grain boundary (TEM): (▲) Mg, (●) Zn.

welded material naturally aged. The most significant differences are that in this work higher zinc and magnesium concentrations were found in grain-boundary regions.

A detailed review is given elsewhere of how over the last 30 years stress corrosion cracking in AlZnMg alloys has been related to microstructural characteristics such as grain-boundary precipitate size and spacing, precipitate-free zone width or solute content, matrix precipitation and slip characteristics [13]. Despite claims to the contrary, no single microstructural parameter has yet been identified as uniquely controlling stress corrosion cracking [14], as it is almost impossible to vary independently the above microstructural parameters. However, with respect to grain-boundary precipitation in general it is well known that stress corrosion cracking is strongly influenced by ageing treatment [15], i.e. extended precipitation times at moderately elevated temperatures (160 °C) are beneficial whereas short low-temperature precipitation treatments are detrimental (120 °C). It should be noted that all AlZnMg alloys are immune to stress corrosion cracking in the as-quenched non-precipitation conditions [16] and all grain boundaries go through an immune to susceptible to highly resistant sequence as grain-boundary precipitation occurs. Alternative mechanisms which have been cited as controlling stress corrosion cracking are related to the relative importance of the grain boundary segregation of zinc [11], magnesium [17] and copper [18, 19], i.e. as these levels are reduced, resistance to stress corrosion cracking is increased.

Although it is not the main concern of this work to examine the mechanism of stress corrosion cracking, which will be discussed in a future publication, it can be seen from the characterization of the white-zone region that the microstructure present does in fact provide the necessary constituents for low stress corrosion cracking resistance, i.e. high solute segregation and grain-boundary precipitation (precipitates can occur as discrete particles, stringers or as agglomerations).

5. Future work

Further work will examine the solute content of grain-boundary regions in the white zone in much greater detail. For fine-scale compositional analysis a scanning transmission electron microscope (STEM) with a probe diameter of less than 2 nm will be used. These findings will be correlated with those of Wall *et al.* [20] who have carried out similar work examining thin foils prepared using electropolishing techniques.

The technique for specimen preparation developed in this study is also very suitable for other investigations, the limiting factor being the cutting ability of the diamond knife. Such investigations may be split into two main types: firstly, because microtomy does not require aggressive electrolytes for specimen preparation it can be used as an alternative method for examining any alloy system which is sensitive to environmental attack (e.g. AlMg alloys), and secondly the technique is very useful for examining areas which require very accurate extraction of samples, e.g. diffusion bonds or crack-tip regions. An example of the accurate positioning of this technique is demonstrated in Fig. 11. Fig. 11a shows an optical picture of stress corrosion cracking, which has occurred in a welded 7017 sample after being exposed to 2% NaCl + 0.5% Na_2CrO_4, pH $3_{(HCl)}$ in a slow strain-rate test. The backscattered electron image (Fig. 11b) reveals that cracking initiated in the weld toe region and propagated via the white zone. Using the cracktip as a marker instead of the microhardness indentations, it was possible to remove thin foil samples from this region. Fig. 11c shows the bulk sample after thin foils have been removed, and Fig. 11d a high-resolution backscattered image exhibiting the intergranular white-zone crack and the adjacent white-zone grain boundaries which appear diffuse and stacked with precipitates.

6. Conclusions

1. The positioning and sectioning technique developed provided an accurate means of studying microstructures from environmentally sensitive regions.

2. Samples prepared by ultramicrotomy have the following advantages. A *bulk section* provides a high-resolution sample suitable for SEM and EPMA obtained without the use of polishing media that can be matched to a corresponding thin foil sample; *thin foils* provide large areas of uniform thickness ideal for microanalysis, and exposure to aggressive solutions during specimen preparation is minimized. The disadvantages of thin foils are that deformation of the thin section restricts the analysis of diffraction information, and some corrosion is observed even with minimal exposure to distilled water.

3. In the white-zone region the grains are essentially larger and more equiaxed than the parent plate. Few precipitates exist within the grains whilst the grain boundaries are stacked with both primary and secondary precipitates. The grain boundaries appear diffuse in backscattered electron imaging (1.2 μm) and microanalysis of thin foils reveals concentrations of

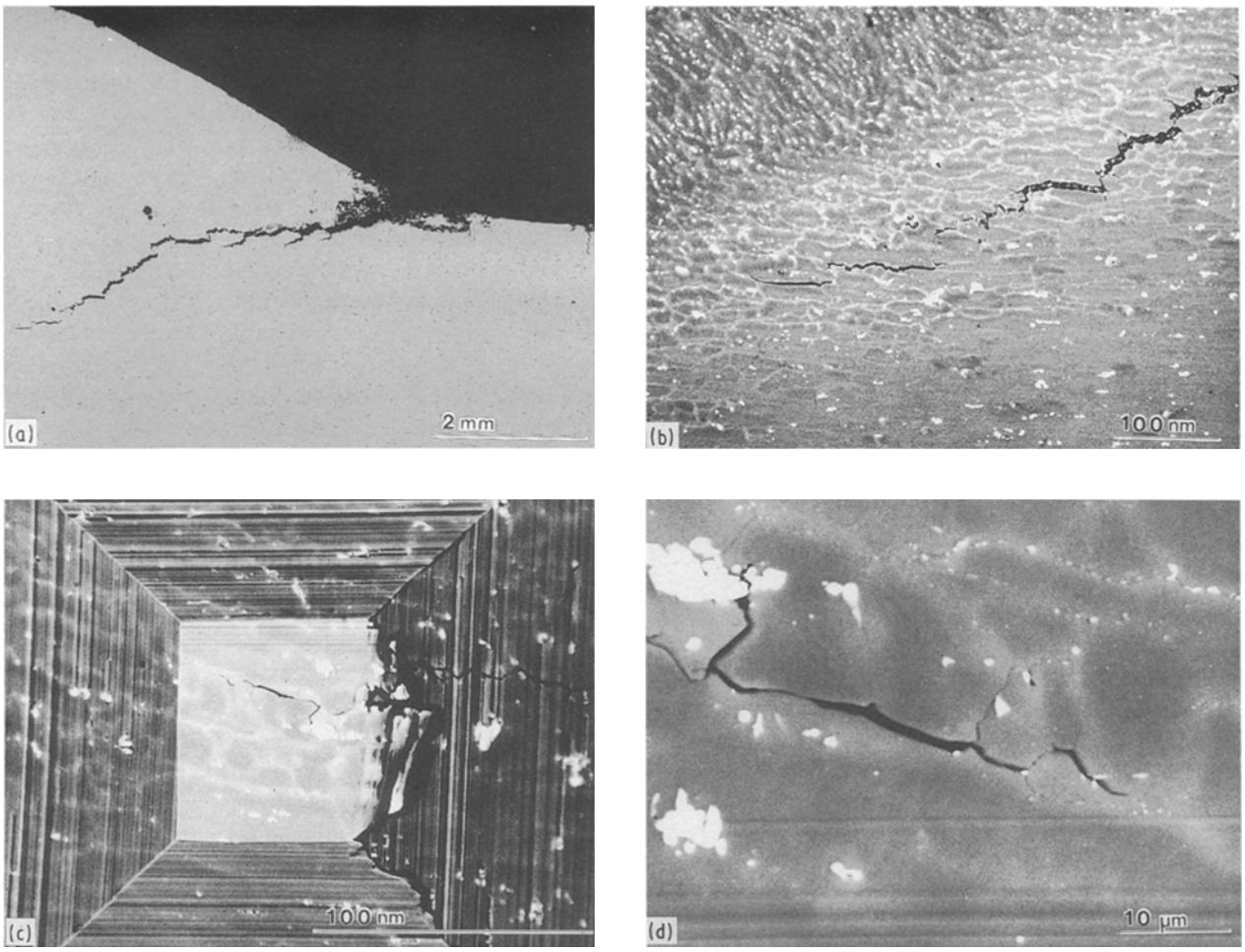

Figure 11 Example of the accurate positioning possible using ultramicrotomy as a technique for specimen preparation: (a) optical micrograph of white-zone crack in 7017 NG61 weldment, (b) backscattered electron image of a white-zone crack, (c) backscattered electron image of microtomed bulk, (d) high-resolution backscattered electron image of microtomed bulk.

zinc, magnesium and copper up to 10, 4 and 0.4 wt %, respectively. Usually zinc, magnesium and copper reach maxima approximately 200 nm from the centre of the grain boundary.

References

1. K. G. KENT, *Metall Rev.* **15** (147) (1970) 135.
2. L. CHAMBERS and D. BAXTER, *Engineer* **223** (1967) 518.
3. M. C. REBOUL, B. DUBOST and M. LASHMERES, *Corros. Sci.* **25** (1985) 999.
4. S. S. BIRLEY, in "Environmental Degradation of Engineering Materials III", edited by M. R. Loutham, R. P. McNitt and R. D. Sisson (Pennsylvania State University, 1987) p. 281.
5. N. J. H. HOLROYD, W. HEPPLES and G. M. SCAMANS, "Corrosion Cracking" (American Society for Metals, Ohio, 1986) p. 291.
6. *Idem*, in "Environmental Degradation of Engineering Materials III", edited by M. R. Loutham, R. P. McNitt and R. D. Sisson (Pennsylvania State University, 1987) p. 293.
7. *Idem.*, European Patent Application 87 308 468.5 (1987).
8. N. J. H. HOLROYD and G. M. SCAMANS, European Patent Application 88 301 227 (1988).
9. H. CORDIER, M. SCHIPPERS and I. J. POLMEAR, *Z. Metallkde* **68** (1977) 280.
10. M. SAJEDAR RAHMAN, H. CORDIER and I. J. POLMEAR, *ibid.* **73** (1982) 589.
11. H. SCHMIEDEL and W. GRUHL, *Metall.* **38** (1984) 32.
12. B. GRZEMBA, H. CORDIER and W. GRUHL, *Aluminium* **63** (1987) 496.
13. N. J. H. HOLROYD, in "Environment Induced Cracking of Metals", edited by R. P. Gangloff and M. B. Ives (NACE, 1990) p. 311.
14. M. O. SPEIDEL, *Met. Trans.* **6A** (1975) 631.
15. D. O. SPROWLS and R. H. BROWN, "Fundamental Aspects of Stress Corrosion Cracking" (NACE, Houston, 1969), p. 466.
16. G. M. SCAMANS, *Aluminium* **57** (1981) 4.
17. J. M. CHEN, T. S. SUN, R. K. VISWANADHAM and J. A. S. GREEN, *Met. Trans.* **8A** (1977) 1935.
18. P. DOIG, P. E. J. FLEWITT and J. W. EDINGTON, *Corrosion* **33** (1977) 217.
19. W. HEPPLES, M. R. JARRETT, J. S. CROMPTON and N. J. H. HOLROYD, in "Environment Induced Cracking of Metals", edited by R. P. Gangloff and M. B. Ives (NACE, 1990) p. 383.
20. M. WALL, J. M. TITCHMARSH and S. S. BIRLEY, presented at AIM Conference on Aluminium for Transport, Milan, November 1987.

Received 4 July 1991
and accepted 29 January 1992